Femtomolar detection of 2,4-dichlorophenoxyacetic acid herbicides *via* competitive immunoassays using microfluidic based carbon nanotube liquid gated transistor

I Putu Mahendra Wijaya ,†[ab] Tey Ju Nie,†[a] Sonu Gandhi,[c] Robin Boro,[c] Alagappan Palaniappan,[a] Goh Wei Hau,[a] Isabel Rodriguez,*[b] C. Raman Suri[c] and Subodh G. Mhaisalkar*[a]

Received 8th September 2009, Accepted 13th November 2009
First published as an Advance Article on the web 16th December 2009
DOI: 10.1039/b918566f

Monitoring of environmental pollutants has become increasingly important due to concern over potential health and environmental impact inflicted by these chemicals. In this contribution, we focus on the development of an all-plastic biosensor comprising laminated single-walled carbon nanotubes as the active element and its conductance modulation in a liquid-gated field effect transistor, as the principle of transduction, for the detection of 2,4-dicholorophenoxy acetic acid (2,4-D) herbicide. The reported biosensor is capable of performing real-time label-free detection of analytes in liquid environment. This biosensor which relies on immunoassay principle for specificity is able to detect down to 500 fM levels of 2,4-D in soil samples.

1. Introduction

Size similarity of nanotubes and most biomolecules allows for the possibility of a mutual interaction at a molecular level[1] that induces specific changes, in both the biomolecules and the nanotubes,[2] thus enabling development of novel biosensing strategies.[3,4] For instance, single-walled carbon nanotubes (SWCNTs) have been employed in the detection of deoxyribonucleic acid (DNA) based on both electrochemical and transistor configuration and detection limits of the order of parts per trillion have been reported.[5,6] Sensors, integrated with microfluidic channels for real-time detection of analytes in liquid media have been reported,[7] however most devices still rely on silicon materials and microlithography techniques for the sensor fabrication and high temperature processes for SWCNT growth.

Environmental pollutants have become a matter of concern in the recent years, due to growing public awareness of the environmental impact and health hazards posed by these pollutants. The wide use of herbicides, fungicides, and pesticides has contributed to the contamination not only of soil, but also ground and surface water as well as the oceans. One such herbicide, 2,4-dichlorophenoxyacetic acid (2,4-D), is widely used for the control of broadleaf weeds in agriculture, and forestry; and has been shown to be very harmful to aquatic life.[8] Conventionally, herbicide analysis is carried out by high-performance liquid chromatography. However, this technique uses bulky and expensive instrumentation and is not suitable for *in situ*, sample testing or prescreening

In this contribution, we focus on the analysis of 2,4-D in soil samples with a SWCNT liquid-gated field effect transistor (LGFET)[9] using a competitive immunoreaction. The LGFET made entirely of plastic, is low cost and the instrumentation required for sensing can be made field-deployable. The proposed immunosensor is also extremely sensitive for the detection of 2,4-D, achieving a limit of detection of 500 fM levels in soil extracted samples.

2. Experimental details

Technical grade 2,4-dichlorophenoxy acetic acid (2,4-D), bovine serum albumin (BSA), *N*-hydroxysuccinimide ester (NHS), *N*′,*N*″dicyclohexylcarbodiimide (DCC), dimethyl formamide (DMF), keyhole limpet hemocyanine (KLH), Freund's completer adjuvant (FCA), Freund's incomplete adjuvant (FIA), goat *anti*-rabbit IgG-HRP conjugate, trifluoroacetic acid (TFA) were purchased from Sigma-Aldrich. 3,3,5,5′-tetramethylbenzidine (TMB) was purchased from Bangalore Genei. Protein A sepharose and sepharose 4 B were procured from Pharmacia. ELISA plates (Nunc F96 MicroWell) were obtained from Maxisorp. Disodium hydrogen phosphate (Na_2HPO_4) and sodium dihydrogen phosphate (NaH_2PO_4) were purchased from Merck. Tween-20 blocking agent and sodium-dodecyl benzene sulfonate (SDDBS) were purchased from Sigma-Aldrich. Poly (dimethyl siloxane) (PDMS) (Sylgard 134) was purchased from DuPont, and carboxylated SWCNTs (2.5 atomic %) were purchased from Cheaptubes. Inc.

The preparation of antibodies against 2,4-D (*anti*-(2,4-D)) has been reported in detail in a previous study[10,11] and schematically shown in Fig. 1 (a). Briefly, the hapten was first prepared by covalently binding the BSA to the 2,4-D with the assistance of DCC + NHS[12] carbodiimide linker molecules, which forms an amide bond between the carboxylic group of the 2,4-D and the surface amino group of the protein. Additionally, the 2,4-D was

[a]*School of Material Science & Engineering, Nanyang Technological University, Singapore, 639798, Singapore. E-mail: i-rodriguez@imre.a-star.edu.sg; subodh@ntu.edu.sg*
[b]*Institute of Materials Research & Engineering, 3 Research Link, 117602, Singapore*
[c]*Institute of Microbial Technology, Sector 39-A, Chandigarh, 160036, India*
† I Putu Mahendra Wijaya and Tey Ju Nie contributed equally in this work.

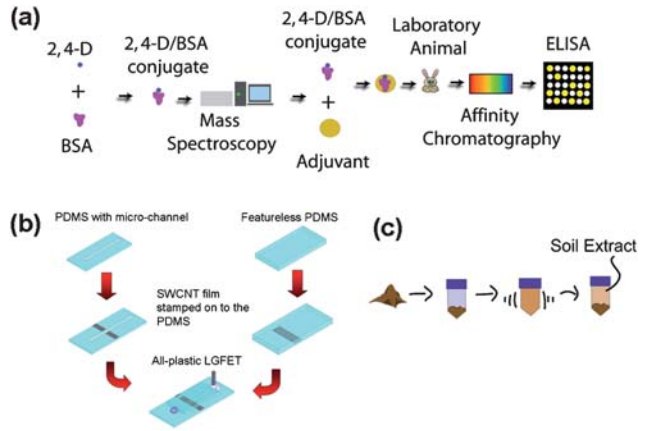

Fig. 1 Protocol for (a) preparation of 2,4-D–BSA conjugate and *anti*-(2,4-D), (b) fabrication process for the SWCNT LGFET. Note that the device comprises of only two materials: PDMS and SWCNT. The liquid-sample is introduced to the device through the microfluidic-channel, and (c) preparation of soil extract.

also conjugated with KLH protein for the coating of ELISA plates with a similar linking strategy, followed by purification of the conjugates using a P10 gel filtration column (Pharmacia). The fractions with maximum protein concentration were collected and stored in aliquots at −20 °C. Subsequently for raising antibodies, six- to eight-weeks old New Zealand white rabbits were immunized subcutaneously with 300–400 μg of the 2,4-D–BSA conjugate emulsified in FCA. Succeeding booster doses were given with FIA at the interval of 21 days. Afterward, the blood was collected and the serum was precipitated. The immunoglobulin (IgG) fractions were purified from the sera using protein-A sepharose column and the bound antibodies were eluted with 0.1M glycine-HCl buffer (pH 2.5). The eluted IgG fractions were pooled and dialyzed against PBS (pH 7.4) at 4 °C, and stored in aliquots at −20 °C. The protocol engaged for generation of *anti*-(2,4-D) from the laboratory animal as reported herein complies with the relevant laws and institutional guidelines, as approved by the Animal Ethics Committee of Institute of Microbial Technology (India) prior to conducting the experiment.

Detailed steps for fabrication of the flexible laminated LGFET have been reported before[9] (Fig. 1 (b)). Briefly, two slabs of PDMS were prepared, one slab was molded with a microfluidic channel and the other was featureless. An aqueous dispersion of SWCNT (0.5 mg ml^{-1}) was prepared by dissolving 25 mg of the nanotubes in 50 ml of SDDBS solution (1% w/v). The solution was sonicated for approximately 2 h for homogenization. The aqueous SWCNT solution was then filtered with an alumina filter (Whatman, 0.1 μm) to form a film of nanotubes on the filter. The resulting SWCNT film was then transfer-printed on to the PDMS slabs through a simple stamping step to form the source–drain electrodes in the slabs carrying the fluidic channel, as well as the transistor channel on the flat slab. The two PDMS slabs were then laminated to form the complete device. The source–drain electrodes and the transistor channel were automatically defined by the microfluidic channel with this device architecture.

The electrical contact is made with the aid of syringe needle tip and silver paint. In specific, the metallic segment of the syringe needle tip is punctured into the dense SWCNT film throughout the thickness of the PDMS to ensure mechanical stability of the contact, and a drop of silver paint is applied at the meeting point of SWCNT film/metal syringe region in fillet configuration to ensure good electrical contact.

Soil samples were obtained from a local plant nursery. To prepare the soil extract, one gram of soil was dispersed in a 50 ml DI water (Millipore). The suspension was then sonicated for 2 h followed by centrifugation at 3000 rpm for 30 min to obtain the soil extract (Fig. 1 (c)).

Transistor measurements were performed by applying a gate bias (V_G) with a function generator (Thurlby Thandar Instrument, TTi TG1304), connected to Ag/AgCl reference electrode (World Precision Instruments). The V_G applied was also monitored with a digital oscilloscope (Agilent DSO3062A). A voltage source/pico-ampere meter module (Keithley 6487) was used to supply the source–drain bias (V_{DS} 10 mV) which measures the source–drain current (I_{DS}) at the same time. All the electrical instruments were synchronized by a personal computer through a general purpose interfacing bus (GPIB) card (National Instrument) and a programming code written in LabVIEW 7.1.

Detection of 2,4-D and *anti*-(2,4-D) antibody was performed through I_{DS}–V_G measurement. To perform direct immuno detection of the 2,4-D, the corresponding antibodies (5 μM) were first covalently attached to the nanotubes to act as the probe molecule *via* DCC + NHS coupling chemistry.[12] Then, free unconjugated 2,4-D (5 μM) was introduced into the microfluidic channel while the I_{DS}–V_G signal was recorded. Similarly, in the case of direct detection of *anti*-(2,4-D), the nanotube surface was first incubated with 2,4-D–BSA conjugate (5 μM) and subsequently, the device was exposed to the antibodies solution (5 μM). The immuno-complex formation in both assays was detected by monitoring the I_{DS}–V_G curve before and after the immunoreaction.

Additionally, kinetic measurements were also performed in triplicate for: (1) Direct immunoassay for the detection of *anti*-(2,4-D) in PB buffer (pH 7.4, 7.3 mS cm^{-1}), (2) competitive immunoassay for the detection of the free 2,4-D in PB buffer (pH 7.4, 7.3 mS cm^{-1}), and (3) real sample analysis for the detection of the free 2,4-D by competitive immunoreaction in soil extract (pH 7, 12 μS cm^{-1}). In all three cases, the 2,4-D–BSA conjugate was used as the probe molecule to capture the *anti*-(2,4-D) antibodies. Logarithmic serial dilutions (5 fM up to 500 μM) of 2, 4-D or *anti*-(2,4-D) were prepared to determine the limit of detection of LGFET. In the direct immunoassay, *anti*-(2,4-D) antibodies at different concentrations was directly applied to the LGFET, which had been initially functionalized with the 2,4-D–BSA conjugate. In the case of competitive immunoassay, a fixed concentration of antibody (50 μM) was first incubated with different concentrations of 2,4-D for 2 h at room temperature (standard solution or soil extract), and subsequently employed for sensitivity studies using LGFET. Selectivity of the device was investigated by exposing a non-pairing protein, such as native BSA to the 2,4-D–BSA conjugate while monitoring the I_{DS}. All measurements were done in triplicates to determine the reproducibility and the standard deviation of the data.

3. Results and discussion

SWCNTs comprise single layers of graphene sheets wrapped into a nano-sized tubular structure, and consequently charge-carriers are confined purely to the surface of the nanotubes. The

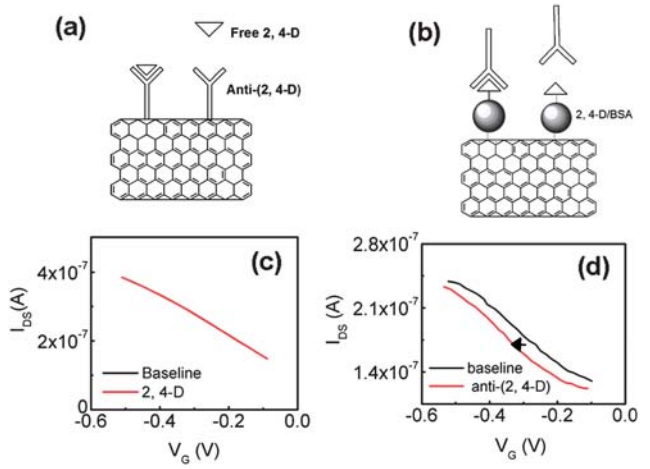

Fig. 2 Schematic of direct assay detection of (a) free 2,4-D and (b) *anti*-(2,4-D), and the corresponding I_{DS}–V_G response ((c) and (d)), respectively. In (a), the 2,4-D and *anti*-(2,4-D) are the target and probe molecule, respectively. In (b), the detection of *anti*-(2,4-D) is carried out using the 2,4-D–BSA conjugate as the probe molecule. The I_{DS}–V_G curve in (c) before (baseline) and after exposure toward the analytes (2,4-D) overlaps.

conductivity of nanotubes is thus very sensitive to the slightest electrostatic disturbances in its surroundings. Biomolecule/SWCNT interactions lead to electrostatic potential disturbance and modulates the nanotube conductance, hence provide a facile transduction mechanism discernible with a LGFET.

In the direct immunoassay format (Fig. 2 (a)), the probe molecule (*anti*-(2,4-D)) is attached on to the nanotube surface, while the free 2,4-D in solution functions as the target molecule. The baseline in transfer characteristic (Fig. 2 (c)) is recorded after the antibody has been attached on to the nanotube, and the unbound SWCNT surface has been passivated with the tween-20 blocking agent. It may be noted that the I_{DS}–V_G curves before and after the 2,4-D exposures completely overlap indicating that the device is not able to detect the immunocomplex formation.

In the immunoassay detection of *anti*-(2,4-D) (Fig. 2 (b)), the 2,4-D–BSA conjugate functions as the probe, while the 2,4-D antibody acts as the target molecule. In contrast to the results obtained in the direct assay, (Fig. 2 (c)), the I_{DS}–V_G characteristic now displays a considerable shift toward the negative V_G values (shown in Fig. 2 (d)).

The differing response levels may be attributed to the large size difference between the free 2,4-D (221.04 g mol^{-1}) and the *anti*-(2,4-D) antibody (1.5×10^4 g mol^{-1}). When used as the probe molecule, bound antibody introduces a large background charge, thus dwarfing the small potential disturbance that the free 2,4-D inflicts upon the immuno-complex formation.

In contrast, the binding of *anti*-(2,4-D) with the 2,4-D–BSA conjugate introduces significant potential disturbance surrounding the nanotubes, and hence leads to shifting of the I_{DS}–V_G curve toward the negative V_G direction (Fig. 2 (d)), indicating that the modulation comes primarily from electrostatic gating. This negative shift normally is associated with the enrichment of positive charge that results when the immunocomplex is formed.

In general, possible sensing mechanisms in LGFETs include electrostatic gating, Schottky barrier, capacitance, and mobility modulation;[13] each of which records a characteristic change in the I_{DS}–V_G curve. Electrostatic gating is associated with a shift in I_{DS}–V_G curve (positive or negative), depending on the charge of the biomolecules binding to the nanotubes. Modulation of the Schottky barrier is characterized by a decrease in I_{DS} at negative V_G bias, and an increase in I_{DS} at positive V_G bias. A change in the capacitance is typified by modulation in the saturation current, whereas mobility changes caused by scattering or other effects of biomolecule/SWCNT interactions show a decrease in gradient under both positive and negative V_G bias.

It can be inferred from the I_{DS}–V_G shift in Fig. 2 (d) that the immunocomplex primarily influences the nanotube through electrostatic gating modulation. Furthermore, the gradient of I_{DS}–V_G curve does not seem to be strongly affected from the immunocomplex formation, indicating that the charge-carrier mobility in the nanotube is unchanged following the immunoreaction.

Prior to the real-time kinetic measurement, the drift characteristic of the LGFET was taken in blank PB buffer as shown in Fig. 3(a). This drift usually is removed off-line before performing analysis to obtain the calibration plot from the kinetic measurement data. The immunocomplex formation in real time was probed by using the LGFET in kinetic mode, which monitors the I_{DS} as a function of time at a fixed V_G (−500 mV) and V_{DS} (10 mV). Hence, in this regard, the non-symmetric I_{DS}–V_G response as observed in Fig. 2 (c) and (d) is also reflected in the kinetic data, because a shift toward negative V_G bias in the I_{DS}–V_G corresponds to a I_{DS} drop in the kinetic measurement.

In the first set, we have tested the device for detection of the antibody (in PB buffer pH 7.4, 7.3 mS cm^{-1}) in direct immunoassay format. In this case, the 2,4-D–BSA conjugate was first covalently immobilized on to the SWCNT using standard carbodiimide linker chemistry. The LGFET was then employed to

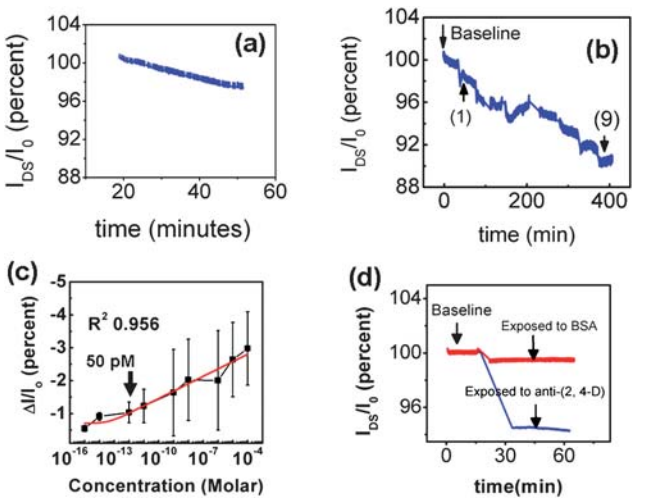

Fig. 3 (a) drift characteristic of the LGFET in blank PB buffer, (b) Kinetic measurement during the immuno complex formation. Concentrations of *anti*-(2,4-D): (1) 5 fM, (2) 50 fM, (3) 5 pM, (4) 50 pM, (5) 5 nM, (6) 50 nM, (7) 5 μM, (8) 50 μM, and (9) 500 μM; to test the sensitivity of the device. (c) Calibration curve resultant from the immunoreaction, and (d) Verification of the specificity of the LGFET showing the response of the sensor when the device is exposed toward native BSA (500 μM) and *anti*-(2,4-D) (500 μM).

capture free antibody in the solution, while measuring the I_{DS} in real-time and keeping the V_G values constant. Fig. 3 (b) reveals the kinetic response from the prepared device upon exposure to *anti*-(2,4-D) antibody solution at increasing concentrations. The I_{DS} here has been normalized to the baseline value (I_o) to remove variability that comes from different numbers of nanotubes on the device. The decrease in I_{DS} indicates that the immunocomplex formation results in enrichment of the positive charge surrounding the nanotube, which is also in support of the data shown in Fig. 2 (d). This positive charge can be attributed to basic amino acid residues, which usually populates the binding pocket of antibodies.

Expectedly, this drop in I_{DS} becomes larger as the antibody concentration in the solution is increased (Fig. 3 (b)). The positive correlation between the I_{DS} drop and the *anti*-(2,4-D) concentration is characteristic of the direct immunoassay tests, because the signal level is directly proportional to the concentration of the antibodies.

The general trend of the I_{DS} drop at different *anti*-(2,4-D) concentrations is noticeable in the calibration curve (Fig. 3 (c)) which represents three kinetic measurement replicates. The calibration data was fitted by the regression equation:[14]

$$\frac{I_{DS}}{I_o} = a - b\log([anti-(2,4-D)] + c) \qquad \text{(Eqn 1)}$$

yielding a correlation factor $R^2 = 0.957$ indicating a good fit between the regression and the underlying data points. The sensitivity of the LGFET in eqn (1) is associated with its gradient, which equals to $\sim$0.21% decade^{-1}, and estimated detection limit of $\sim$ 50 pM (50 part-per-trillion) for the case of detection of *anti*-(2,4-D) in PB buffer.

The selectivity of the LGFET was also investigated by exposing the device toward a non-pairing protein, such as native BSA. Fig. 3 (d) shows that the I_{DS} drop only slightly upon exposure to the native BSA, also confirming the effectiveness of tween-20 as the blocking agent which prevents attachment of excess biomolecules directly to CNTs and potentially interfering with the sensing response.

As discussed earlier (Fig. 2 (c)), the detection of free 2,4-D using direct immunoassay protocol is not possible due to its small size as compared to the *anti*-(2,4-D) which results in negligible electrostatic changes produced by the antigen molecule. An alternative to detect the free 2,4-D in solutions is through a competitive immunoassay protocol. For this, a fixed concentration of antibody (50 μM) was mixed with a series of free 2,4-D solutions differing in concentration. Upon injection into the LGFET, the free 2,4-D molecule competes with the 2,4-D–BSA conjugate to bind with the *anti*-(2,4-D) antibody in solution (Fig. 4 (a)). Therefore, the larger the concentrations of free 2,4-D, the less the free binding sites of *anti*-(2,4-D) antibody that bind with the 2,4-D–BSA conjugate. Hence, the competitive assay protocol yields a calibration plot that is inversely proportional to the concentration of free 2,4-D in solution. The kinetic response (Fig. 4(b)), however, is similar to direct immunoassay protocol (Fig. 3(b)), because in both cases, the device detects binding of *anti*-(2,4-D) antibody to the 2,4-D–BSA conjugate.

The inverse relationship between current and concentration of 2,4-D is also observed in the calibration curve (Fig. 4 (c)) which is derived from three kinetic measurement replicates. As described

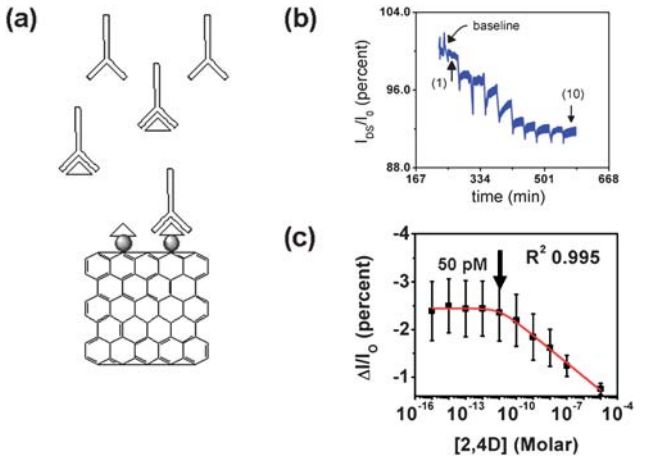

Fig. 4 (a) Schematic of a competitive immunoassay. In this protocol, the free 2,4-D is detected indirectly. (b) Kinetic response from the LGFET upon exposure of free 2,4-D at different concentrations: (1) 50 μM, (2) 500 nM, (3) 50 nM, (4) 5 nM, (5) 500 pM, (6) 50 pM, (7) 5 pM, (8) 500 fM, (9) 50 fM, and (10) 5 fM in PB buffer (pH 7.4, 7.3 mS cm^{-1}) (c) Calibration curve resultant from the immunoreaction.

earlier (eqn (1)), the $R^2 = 0.995$ indicates excellent regression fit with sensitivity of $\sim$0.33% decade^{-1}, and a 2,4-D detection limit of $\sim$50 pM (50 part-per-trillion) - which is much lower than the World Health Organization (WHO) established maximum residual level of 2,4-D concentration in drinking water [15] at 500 nM (500 part-per-billion) levels.

In a third set of experiments, the competitive immunoassay was employed to detect the free 2,4-D in the real sample of soil extract with the LGFET. The pH and the conductivity of the soil extract were found to be in the range of 7, and 12 μS cm^{-1}, respectively. This indicates that even though the soil extract has a pH, similar to that of lab condition (pH 7.4, and conductivity 7.3 mS cm^{-1}), the ionic-strength of the extract is much lower than those tested in the lab.

It may be noted from the kinetic response and calibration plots (Fig. 5 (a,b)) that the change in I_{DS} is almost similar to those observed in Fig. 4 (b) and (c), except that it is somewhat larger in

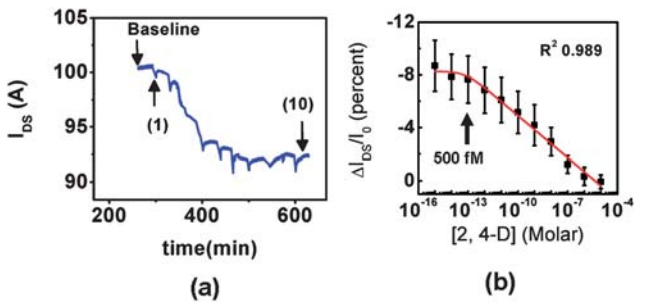

Fig. 5 (a) Kinetic measurement upon exposure to the free 2,4-D in soil extract in competitive immunoassay format. The I_{DS} decreases upon exposure toward the free 2,4-D with different concentrations: (1) 5 μM, (2) 500 nM, (3) 50 nM, (4) 5 nM, (5) 500 pM, (6) 50 pM, (7) 5 pM, (8) 500 fM, (9) 50 fM, and (10) 5 fM. (b) The calibration curve shows inverse relationship between the level of signal and the free 2,4-D concentration, typical for competitive immunoassay. The calibration curve is obtained from three replicates of kinetic measurements.

the case of soil extract. This slight amplification is attributable to the lower ionic-strength (12 μS cm^{-1}) of the soil extract as compared to PB buffer solution (7.3 mS cm^{-1}). In aqueous solutions, the polar and/or charged surface of biomolecules attracts counter-ions from their surroundings. These counter-ions screen the stray potential which originates from the biomolecules and is required to disturb the conductance of the SWCNTs. In higher ionic-strength solutions, this screening process is more effective than in lower-ionic strength and hence, the signal in LGFETs is inversely proportional to the ionic-strength of the solution,[16] and probably is the reason why the change in I_{DS} is slightly larger in the case of soil extract than in PB buffer.

The correlation factor R^2 of 0.989 as extracted from eqn (1) and the sensitivity of 0.94% $decade^{-1}$ is higher than the previous two cases and the limit of detection is estimated at 500 fM (0.5 part-per-trillion). The improvement in the sensitivity and limit of detection over the case of 2,4-D detection in PB buffer is a direct consequence of the larger I_{DS} drop observed in the soil extract.

4. Conclusion

In this contribution, we have developed a LGFET microfluidic based biosensor and methodologies, direct, indirect and competitive immunoassays for the detection of a commonly used herbicide 2,4-D. The detection as extracted from the drain current response of the LGFETs yielded a real-time, label-free detection of free 2,4-D molecules with extremely low detection limits of ~500 fM (0.5 part-per-trillion) and 50 pM (50 part-per-trillion) in soil extract and buffer solution, respectively. These detection limits are much lower than the maximum residual limit of 500 nM (500 part-per-billion) for the 2,4-D established by the WHO in drinking water.

The instrumentation and technology developed is simple and low cost, hence, has the potential for *in situ* analysis of environmental samples including detection of waterborne toxins or in the medical field to replace some of the immunoassay based diagnostic methodologies currently performed.

References

1 K. Balasubramanian and M. Burghard, *J. Mater. Chem.*, 2008, **18**, 3071–3083.
2 I. P. M. Wijaya, S. Gandhi, T. J. Nie, N. Wangoo, I. Rodriguez, G. Shekhawat, C. R. Suri and S. G. Mhaisalkar, *Appl. Phys. Lett.*, 2009, **95**, 073704.
3 K. Bestman, J.-O. Lee, F. G. M. Wiertz, H. A. Heering and C. Dekker, *Nano Lett.*, 2003, **3**, 727–730.
4 G. Grunner, *Anal. Bioanal. Chem.*, 2005, **384**, 322–325.
5 J. Li, H. T. Ng, A. Cassell, W. Fan, H. Chen, Q. Ye, J. Koehne, J. Han and M. Meyyappan, *Nano Lett.*, 2003, **3**, 597–602.
6 A. Star, V. Joshi, T.-R. Han, M. V. P. Altoe, G. Gruner and J. F. Stoddart, *Org. Lett.*, 2004, **6**, 2089–2092.
7 W. Y. Ng, S. Goh, Y. C. Lam, C. Yang and I. Rodriguez, *Lab Chip*, 2009, **9**, 802–809.
8 E. O. Oruc, Y. Sevgiler and N. Uner, *Comp. Biochem. Physiol., Part C: Toxicol. Pharmacol.*, 2004, **137**, 43–51.
9 J. N. Tey, I. P. M. Wijaya, Z. Wang, W. H. Goh, A. Palaniappan, S. G. Mhaisalkar, I. Rodriguez, S. Dunham and J. A. Rogers, *Appl. Phys. Lett.*, 2009, **94**, 013107.
10 Z. Liu, S. M. Tabakman, Z. Chen and H. Dai, *Nat. Protoc.*, 2009, **4**, 1372–1381.
11 K. V. Singh, J. Kaur, G. C. Varshney, M. Raje and C. R. Suri, *Bioconjugate Chem.*, 2004, **15**, 168–173.
12 W ten Hoeve, H. Wynberg, W. T. Jones, D. Harvey, G. B. Ryan and P. H. S. Reynolds, *Bioconjugate Chem.*, 1997, **8**, 257–266.
13 I. Heller, A. M. Janssens, J. Mannik, E. D. Minot, S. G. Lemay and C. Dekker, *Nano Lett.*, 2008, **8**, 591–595.
14 D. A. Ratkowsky, *Handbook of nonlinear regression models*, Marcel Dekker, Inc., New York, 1990.
15 E. Brillas, J. C. Calpe and J. Casado, *Water Res.*, 2000, **34**, 2253–2262.
16 A. Poghossian, A. Cherstvy, S. Ingebrandt, A. Offenhausser and M. J. Schooning, *Sens. Actuators, B*, 2005, **111–112**, 470–480.

